Chemical Engineering Science 79 (2012) 19–28

Contents lists available at SciVerse ScienceDirect

Chemical Engineering Science

journal homepage: www.elsevier.com/locate/ces

Review

A physical model for huge wave movement in gas–liquid churn flow

Ke Wang [a], Bofeng Bai [a,*], Jiahuan Cui [a], Weimin Ma [b]

[a] State Key Laboratory of Multiphase Flow in Power Engineering, Xi'an Jiaotong University, Shaanxi, 710049, China
[b] Royal Institute of Technology (KTH), Stockholm, Sweden

HIGHLIGHTS

- We modeled the huge wave growth and levitation process in churn flow.
- The results agreed well with existing experimental measurements.
- We explained the flooding was a character throughout churn flow regime.
- Wave properties are different from those in annular flow.

ARTICLE INFO

Article history:
Received 5 December 2011
Received in revised form
4 April 2012
Accepted 8 May 2012
Available online 18 May 2012

Keywords:
Churn flow
Flooding
Multiphase flow
Interface
Mathematical modeling
Numerical analysis

ABSTRACT

A complete knowledge of the huge wave in churn flow is of great importance for the characterization of its entrainment. Huge wave in churn flow is experimentally identified as a highly disturbed wave; however, no specific model is available for this particular wave. Based on the force balance over the wave, we established an analytical model to study its growth and levitation and analyzed the effects of the parameters (including gravity, pressure force of gas and liquid, wall shear stress and interfacial shear stress) on the wave and the gas and liquid flow field. We proposed that the boundary layer in liquid film is more likely to be turbulent rather than laminar and the gas pressure force is the most influential factor. The proposed model was verified qualitatively and quantitatively. We hence theoretically concluded that the churn flow is characterized by the flooding of the film, the flow reversal is attributed to the transition to the annular flow and the pressure gradient decreases with the increase of the gas flow rate. These findings provided insight into the distinction between the churn flow and the annular flow. The wave properties (amplitude and velocity) were analyzed in detail and the churn/annular transition occurred at $U^*=1.12$. The model helps understand the droplet entrainment in churn flow which is essential for the development of mechanistic models to predict the dryout condition.

Contents

* Corresponding author. Tel.: +86 29 82665316; fax: +86 29 82669033.
E-mail address: bfbai@mail.xjtu.edu.cn (B. Bai).

0009-2509/$ - see front matter © 2012 Elsevier Ltd. All rights reserved.
http://dx.doi.org/10.1016/j.ces.2012.05.011

1. Introduction

Churn flow normally occurs in vertical or nearly vertical pipes and appears a highly disturbed flow of gas and liquid. It features interfacial waves termed as huge waves (Sekoguchi and Takeishi, 1989) over a liquid film, as well as a sudden increase in pressure gradient at the formation of churn flow following the breakdown of slug flow (Owen, 1986); the pressure gradient decreases with the further increase in gas flow rate, but eventually increases again as the flow enters the annular regime. The reversal in the liquid flow direction occurs as the dimensionless superficial gas velocity U^* approximates unity (Wallis, 1969; Hewitt et al., 1985):

$$U^* = u_{sg}\sqrt{\frac{\rho_g}{gd_T(\rho_l-\rho_g)}} \tag{1}$$

where u_{sg}, d_T, g, ρ_l and ρ_g are gas superficial velocity, hydraulic diameter, gravitational acceleration, liquid density and gas density, respectively.

However, churn flow, bounded by the slug and the annular flow regimes, is not unanimously defined. Zuber and Findlay (1965) took it as a type of bubbly flow, while Taitel et al. (1980) considered it as a developing slug flow. Hewitt and Hall-Taylor (1970) proposed that churn flow was an intermediate flow regime between slug and annular flow, occurring after the breakdown of slug flow as velocity increased. Hewitt and Hall Taylor's definition is generally accepted and is thus adopted in the present study.

The flooding of the liquid film surrounding the Taylor bubble is attributed to the transition from slug flow to churn flow (Wallis, 1969; McQuillan et al. (1985); Govan et al. 1991; Jayanti and Hewitt, 1992; Hewitt and Jayanti, 1993; Jayanti et al., 1993). During this process, huge waves, also referred to as large wave or flooding-type wave, are observed traveling upwards with falling film regions between the waves (Hewitt et al., 1985; Barbosa et al., 2001). A complete knowledge of the huge wave in churn flow is of great importance for the characterization of its entrainment. However, thorough studies on the huge wave are relatively few, though their significance for the studies on the countercurrent flow is obvious: The origin of the huge wave in churn two-phase flow is believed to be similar to that which causes the flooding in a countercurrent two-phase flow, indicating the occurrence of churn flow can be characterized by its capability of forming huge waves; to a large extent, such a countercurrent flow occurs in many applications such as gas lift in chemical engineering and emergency cooling of the reactor core in case of the loss of coolant. Recently, Ahmad et al. (2010) claimed that in a dryout model it was more justifiable to integrate entrainment and deposition processes in the churn flow than in the annular flow in a channel. Therefore, researches on the huge wave in churn flow are crucial for the development of mechanistic models to predict the dryout condition.

Motivated by the extensive application of the huge wave in churn flow, some physical models have been developed, including a reliable analysis of the mechanism of churn flow based on force analysis (Barbosa et al., 2001), a volume of fluid (VOF) method for the levitation process of the huge wave typical in churn flow and the effects of physical properties on interfaces conversion (Da Riva and Del Col, 2009). It should be noted that previous studies in this field have their reference significance. However, to our best knowledge, there is no mathematical model for the study of the variation of the forces acting on the huge wave, and of the properties of the huge wave in churn flow.

To simulate the huge wave in churn flow, two key issues need to be addressed. First, the huge wave has to be described with appropriate terms concerning its shape. In practice, the interfacial wave in churn flow is hard to measure. Experimental studies (though not many) on the wave shape in annular flow (Wang et al., 2004a, 2004b; Han et al., 2006; Omebere-Iyari and Azzopardi, 2007; Hazuku et al., 2008) indicated that the interfacial wave very likely had a log-normal distribution. However, calculations could be quite complicated with such a wave shape. McQuillan et al. (1985) proposed a hemispherical shape to simplify the calculation, which was also adopted by Da Riva and Del Col (2009). Unquestionably, this simplification makes the calculation much easier; however, the hemispherical shape is a far cry from the real wave and errors will be inevitably resulted. Therefore, a simpler wave shape featuring the general characteristics has to be employed. The shape for the standing wave on the falling film was estimated as sinusoidal by Shearer and Davidson (1965) and it was verified by Hewitt et al. (1985) that the assumed wave was similar in shape to the measured one. This sinusoidal wave was also adopted by Holowach et al. (2002) and Barbosa et al. (2001) and provided a more simplified approach for the quantification of the force balance. Accordingly, in our study we employed a sinusoidal shape to simplify the modeling. Second, a detailed analysis about the forces acting on the wave in different degrees is required to determine the wave behavior. Hence, the analysis on both the gas and liquid flow field is necessary.

Based experimentally on the findings of our study (Wang et al., 2011), we established a physical model in this paper for the investigation into the wave levitation in churn flow. We analyzed in detail the boundary layer in the wavy region and the variations of the gas flow field over a wave and discovered the impact of the forces including gravity, gas pressure and liquid pressure, wall shear stress and interfacial shear stress. The present model was qualitatively and quantitatively verified by our experimental results. On the basis of this mathematical model, we investigated the variations of the pressure gradient and the forces during the moving process and the wave properties including amplitude and velocity. The model developed here helps understand the transition from churn flow to annular flow and the mechanism of the entrainment in churn flow which is essential for the development of mechanistic models to predict the dryout condition.

2. The mathematical model

2.1. Control volume

In the experimental study of churn flow (Barbosa et al., 2001; Wang et al., 2011), the liquid flows smoothly into the pipe through the porous section and forms a downwards liquid film near the wall. An interfacial wave generates at the base of the porous section and is taken as the control volume in the present modeling, as is shown in Fig. 1. The gas is assumed to be inviscid and separated from the liquid phase by a vertical interface on which the waves move with the velocityU_w. The mass and momentum conservation principles for

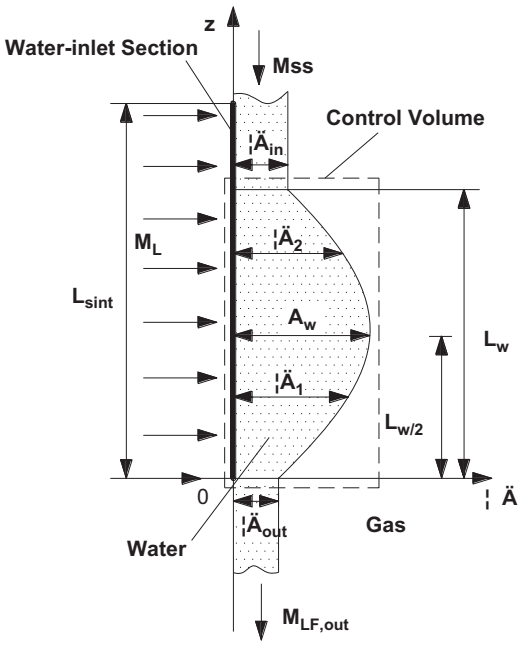

Fig. 1. Sketch of control volume.

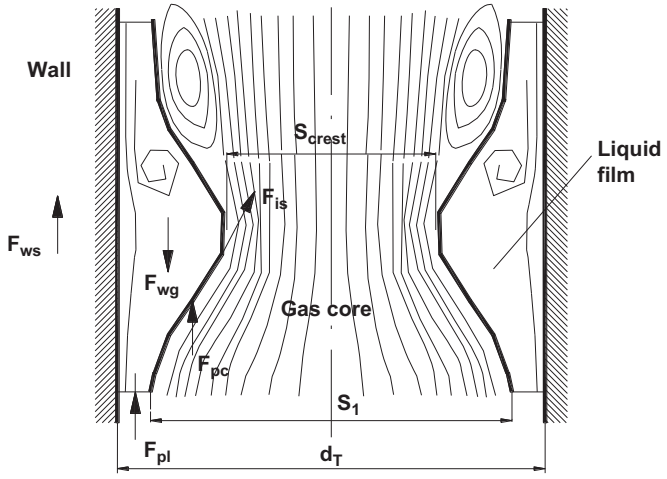

Fig. 2. Force balance for a control volume.

wave development can be described as follows:

$$\sum F = \rho_l \frac{d}{dt}(U_w V_w) - (U_{LF,in}\dot{M}_{LF,in} - U_{LF,out}\dot{M}_{LF,out}) \tag{2}$$

$$\rho_l \frac{dV_w}{dt} = \dot{M}_{LF,in} - \dot{M}_{LF,out} \tag{3}$$

where ΣF, V_w, $U_{LF,in}$, $U_{LF,out}$, $\dot{M}_{LF,in}$, $\dot{M}_{LF,out}$ are the resultant force acting on the wave in the vertical direction, the wave volume, the velocity of the liquid film at the inlet and at the outlet of the control volume, the liquid mass flow rate at the inlet and at the outlet of the wave, respectively. The wave velocity can be calculated as:

$$\frac{d}{dt} z = U_w \tag{4}$$

where z is the wave traveling distance in the axial direction.

The calculation of the wave volume is conditioned on the assumption of a sinusoidal wave which endures as the wave grows. The arbitrary thickness of liquid filmδcan be calculated as:

$$\delta = \begin{cases} \delta_1, 0 \le z \le L_w/2 \\ \delta_2, L_w/2 \le z \le L_w \end{cases} \tag{5}$$

$$\delta_1 = \frac{1}{2}\left[(\delta_{out} + A_w) + (\delta_{out} - A_w)\cos\frac{2\pi z}{L_w}\right] \tag{6}$$

$$\delta_2 = \frac{1}{2}\left[(\delta_{in} + A_w) + (\delta_{in} - A_w)\cos\frac{2\pi z}{L_w}\right] \tag{7}$$

whereδ_{in}, δ_{out}, A_w and L_w are the liquid film thicknesses at the inlet and at the outlet of the wave, the wave amplitude and the wave length, respectively. The ratio of the wave length to the amplitude is taken to be consistent as the wave remains unchanged in its shape. Since relevant experimental data about wave amplitude and wave length are not available in great abundance in references and according to the experimental study by Wang et al. (2011) the ratio of the wave length to the amplitude ranges from 4.2 to 5.1,in the present work their ratio is assumed as $L_w/A_w = 5$ for the sake of the simplification of the calculations. With L_w/A_w ranging from 4 to 5, the calculations show little difference for the final results.

Therefore, the wave volume and its time derivative can be calculated as follows:

$$\begin{aligned} V_w &= \pi\left[\int_0^{L_w/2}(d_T - \delta_1)\delta_1 dz + \int_{L_w/2}^{L_w}(d_T - \delta_2)\delta_2 dz\right] \\ &= \frac{1}{4}\pi d_T L_w(2A_w + \delta_{out} + \delta_{in}) - \frac{1}{8}\pi L_w\left[(A_w + \delta_{in})^2\right. \\ &\quad \left. + (A_w + \delta_{out})^2\right] - \frac{1}{16}\pi L_w\left[(\delta_{in} - A_w)^2 + (\delta_{out} - A_w)^2\right] \end{aligned} \tag{8}$$

$$\frac{dV_w}{dt} = C_1\frac{d}{dt}A_w + C_2\frac{d}{dt}\delta_{in} + C_3\frac{d}{dt}\delta_{out} \tag{9}$$

where,

$$C_1 = \frac{5}{16}\pi(16d_T A_w + 4d_T\delta_{in} + 4d_T\delta_{out} - 18A_w^2 - 4\delta_{in}A_w - 4\delta_{out}A_w - 3\delta_{in}^2 - 3\delta_{out}^2) \tag{10}$$

$$C_2 = \frac{5}{16}\pi A_w(4d_T - 2A_w - 6\delta_{in}) \tag{11}$$

$$C_3 = \frac{5}{16}\pi A_w(4d_T - 2A_w - 6\delta_{out}) \tag{12}$$

The liquid film thicknesses at the inlet and the outlet of the wave can be calculated by Nusselt film theory (Nusselt, 1916):

$$\delta_{in(out)} = \left[\frac{3\eta_l \dot{M}_{LF,in(out)}}{\pi d_T \rho_l g(\rho_l - \rho_g)}\right]^{1/3} \tag{13}$$

whereη_l and $\dot{M}_{LF,in(out)}$are the liquid viscosity and the liquid film mass flow rate at the inlet and the outlet of the control volume, respectively.

With the reference to the experiments under churn flow conditions (Barbosa et al., 2001; Wang et al., 2011), the inlet section is designed with uniformly distributed holes so that the water flows into the channel smoothly. The liquid flow rates at the inlet and the outlet of the control volume $\dot{M}_{LF,in(out)}(z)$ vary with distance and are assumed to be linear with the wave traveling upwards to the top of the inlet section. The wave forming at the liquid inlet continues growing until it reaches the amplitude large enough to move upwards. Waves generate at the bottom of the water inlet section, where the mass flow rate at the inlet of the wave volume is the greatest. When the wave travels through the top of the water inlet section, mere the falling

liquid film enters the control volume.

$$\dot{M}_{LF,in}(z) = (1-E)\dot{M}_L - \frac{[(1-E)\dot{M}_L - \dot{M}_{SS}]z}{L_{\text{sint}}} \tag{14}$$

$$\dot{M}_{LF,out}(z) = \dot{M}_{out} - \frac{(\dot{M}_{out} - \dot{M}_{SS})z}{L_{\text{sint}}} \tag{15}$$

where $\dot{M}_{out}$, $\dot{M}_{SS}$, $\dot{M}_L$, L_{sint} and E are the liquid mass flow rate at the outlet of the experimental system, the liquid film mass flow rate, the total liquid mass flow rate, the length of water inlet section and the entrained fraction, respectively. The conventional measurement for the liquid film mass flow rate between the waves in churn flow could not be applied due to its chaotic nature. Barbosa et al. (2001) assumed $\dot{M}_{SS}$as a certain proportion of $\dot{M}_L$, ranging from 5∼15%, and concluded that the values made little difference to the final results. Azzopardi and Wren (2004) analyzed the experimental data of Assad et al. (1998) and suggested that 7% of the liquid was in the base film, 71% in the huge waves and 22% in the drop form. Therefore, $\dot{M}_{SS}$is taken as 10% of the total liquid mass flow rate $\dot{M}_L$in this paper. Moreover, part of the liquid will be entrained into the gas core during the wave movement. Azzopardi and Wren (2004) measured the entrained fraction in air/water churn flow by using T-junction at the pressure of 1∼3 bar. They proposed an empirical formula for the entrained fraction with a mean error of 3% and a standard deviation of 11.7%. This empirical formula is adopted in our present study:

$$\begin{aligned} E &= 0.47u_{sg}^{0.16}u_{sl}^{0.35} \quad for\ u_{sg} < 5m/s \\ E &= 0.6u_{sl}^{0.35} \quad for\ u_{sg} > 5m/s \end{aligned} \tag{16}$$

2.2. Forces on control volume

The forces exerting on the control volume are illustrated in Fig. 2. The effects of the gravity ($\vec{F}_{wg}$), the pressure variations in gas core and liquid film ($\vec{F}_{pc}$,$\vec{F}_{pl}$), the interfacial shear stress ($\vec{F}_{is}$) and the wall stress ($\vec{F}_{ws}$) are taken into account.

The resultant force acting on the control volume can be described as:

$$\Sigma F = \vec{F}_{pc} + \vec{F}_{pl} + \vec{F}_{ws} + \vec{F}_{wg} + \vec{F}_{is} \tag{17}$$

2.2.1. Gravitational force

Based on the estimation of the wave volume, the gravitational force on the wave can be calculated as:

$$F_{gw} = (\rho_l - \rho_g)gV_{\text{w}} \tag{18}$$

2.2.2. Pressure variations in the gas core

Fig. 3 shows the simulation results of the pressure variation at the centerline and wavy wall reported by Jayanti et al. (1996). The minimum pressure along the centerline of the pipe occurs at a point farther downstream from the wave crest. The pressure then recovers but with a net loss in pressure down the wave. The pressure on the wavy wall (interface) increases prior to the wave crest, but decreases dramatically at the crest. The flow then separates and afterwards the pressure varies little before the flow reattaches to the wavy wall after which it recovers rapidly its steady value.

Assuming that the gas flow separates immediately after the crest of the wave, the pressure exerting on the leeward side of the wave is consistent with that in the wave crest P_{crest}. The pressure drop Δp acting on the control volume between the windward $P_{c,in}$ and the leeward sides of the wave can be roughly estimated by

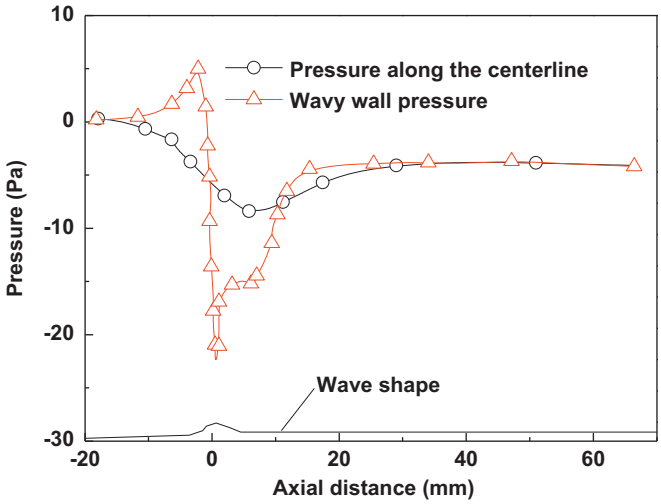

Fig. 3. Variation of static pressure in the channel (Jayanti et al., 1996).

the Bernoulli equation as:

$$\Delta P = P_{c,in} - P_{crest} = \frac{\rho_c}{2}U_c^2\left[\left(\frac{S_1}{S_{crest}}\right)^2 - 1\right] \tag{19}$$

$$S_1 = \frac{\pi}{4}(d_T - 2\delta_{out})^2 \tag{20}$$

$$S_{crest} = \frac{\pi}{4}(d_T - 2A_w)^2 \tag{21}$$

whereS_1, S_{crest},ρ_c and U_c are the cross-sectional area for the gas flow at the wave windward and at the wave crest, the density of the gas core, and the average velocity of the gas core before the windward side, respectively. The density of the gas core ρ_c and the average velocity of the gas core $U_c$are both defined in terms of the pure gas and entrained droplets:

$$\rho_c = \frac{\dot{M}_{LE} + \rho_g G_g}{\dot{M}_{LE}/\rho_l + G_g} \tag{22}$$

$$U_C = \frac{\dot{M}_{LE}/\rho_l + G_g}{S_1(1-(2\delta_{out}/d_T))^2} \tag{23}$$

where $G_g$is the gas flow rate.

Therefore, the force exerting on the wave due to the pressure variations in the gas core can be estimated by multiplying the pressure drop Δp by the projected area of the wave surface onto the radial planeS_p:

$$F_{pc} = \Delta p S_p \tag{24}$$

$$S_p = \pi A_w(d_T - A_w) \tag{25}$$

2.2.3. Pressure variations in the liquid film

The force acting on the top and bottom of the wave can be calculated as follows:

$$F_{pl} = P_{l,in}S_{LF,in} - P_{l,out}S_{LF,out} \approx \frac{1}{2}(P_{l,in} - P_{l,out})(\delta_{in} + \delta_{out})\pi d_T \tag{26}$$

where $P_{l,in}$, $P_{l,out}$, $S_{LF,in}$ and $S_{LF,out}$ are the pressure acting on the outlet and on the inlet of the wave, the cross-sectional area of the top and of the bottom of the wave, respectively.

According to a rough estimation by the Nusselt film theory, the liquid film at the inlet and the outlet of the control volume is quite thin ($\times 10^{-4}$ m). Based on the analysis on the stability of the interface between the liquid and the gas, the pressures of the gas

core and the liquid film have the following relations (Wallis, 1969):

$$P_l - P_c = -\sigma \frac{d^2\delta}{dy^2} \tag{27}$$

where $\sigma$is the surface tension. Therefore, the pressure difference between the top and bottom of the wave is:

$$P_{l,in} - P_{l,out} = (P_{c,in} - P_{c,out}) + \sigma\left(\left.\frac{d^2\delta}{dy^2}\right|_{y=0} - \left.\frac{d^2\delta}{dy^2}\right|_{y=Lw}\right)$$
$$= \Delta P + \sigma\left(\left.\frac{d^2\delta}{dy^2}\right|_{y=0} - \left.\frac{d^2\delta}{dy^2}\right|_{y=Lw}\right) = \Delta P + \frac{2\pi^2}{L_w^2}\sigma(\delta_{out} - \delta_{in}) \tag{28}$$

where ΔP is the gas pressure difference which can be calculated by Eq. (19).

2.2.4. Wall shear stress

In the churn flow in a vertical channel, the flow near the wall is more complex than that in the annular flow. The liquid film between the interfacial waves is very thin and flows downwards. Hewitt et al. (1985) assumed that the boundary layer is laminar as the mixing zone is short, and the boundary layer length is equal to the wave length, which was accepted by Barbosa et al. (2001). However, as they admitted, an obvious liquid circulation exists in the wave region and gives rise to a peak in the velocity profile. Also, our calculation shows that the Reynolds number of liquid film is more likely turbulent rather than laminar ($Re > 2900$). Therefore, we propose that the boundary layer in the liquid film is more justifiably turbulent rather than laminar. Since the thickness of the liquid film between the interfacial waves seems to have the same order ($\times 10^{-4}$ m) as the thickness of the viscous sublayer in the single turbulent liquid flow, we assume that the velocity gradient at the interface in churn flow is zero, which is similar to that in the single liquid phase flow where the velocity gradient approximates zero quickly within a certain distance away from the wall. Hence, the velocity profile in the turbulent flow of the single liquid phase is used to determine the wall shear stress in churn flow.

Based on the boundary layer theory in single liquid phase flow, the calculation of the wall shear stress can be expressed as:

$$F_{ws} = \int_{z-L_w/2}^{z+L_w/2} f_\tau dz \tag{29}$$

$$f_\tau = \pi d_T \tau_{wall} = \frac{\pi {d_T}^2}{2r_\delta}\tau_\delta \tag{30}$$

$$\tau_\delta = \tau_{tur} + \tau_{lam} \tag{31}$$

where τ_{wall},τ_δ,r_δ, and f_τ are wall shear stress, shear stress at the interfaces in single liquid phase flow, distance from the centerline, and wall stress per length, respectively. The shear stress τ_δ can be taken as the sum of Reynolds stress τ_{tur} and laminar shear stressτ_{lam}, both of which depend on the velocity gradient of the mean-time-average velocity $\bar{u}$ along the distance y from the wall $d\bar{u}/dy$.

The velocity distribution within the smooth pipe in single liquid phase flow can be described as:

$$\frac{\bar{u}}{U} = \left(\frac{y}{R}\right)^{1/n} = \left(1 - \frac{r}{R}\right)^{1/n}, \quad \mathrm{Re} > 2100 \tag{32}$$

where U and R are the velocity at the pipe center and the pipe radius, respectively.

Therefore,

$$\frac{d\bar{u}}{dy} = \frac{U}{nR}\left(\frac{R}{y}\right)^{\frac{n-1}{n}} \tag{33}$$

In addition, the cross-sectional average velocity in the pipe can be calculated as:

$$\bar{V} = \frac{1}{\pi R^2}\int_0^R 2\pi r\bar{u}dr = \frac{2n^2}{(n+1)(2n+1)}U \tag{34}$$

Therefore,

$$\mathrm{Re} = \frac{\rho_l \bar{V} d_T}{\eta} = \frac{\rho_l d_T}{\eta}\frac{2n^2}{(n+1)(2n+1)}\frac{\bar{u}_\delta}{(1-2(r_\delta/d_T))^{1/n}} \tag{35}$$

where $\bar{u}_\delta$is the local velocity at the interface in single liquid phase flow.

According to the experimental data reported by Munson et al. (1990), a correlation relating Re and $n$can be obtained as

$$\mathrm{Re} = 1.404n^{6.292} - 1.510 \times 10^5 \tag{36}$$

By solving Eqs. (29), (30), and (32), the wall shear stress can be expressed as:

$$f_\tau = \frac{\pi d_T^2}{2r_\delta}\left\{\rho_l l_m^2\left[\frac{U}{nR}\left(\frac{R}{y}\right)^{\frac{n-1}{n}}\right]^2 + \mu\frac{U}{nR}\left(\frac{R}{y}\right)^{\frac{n-1}{n}}\right\} \tag{37}$$

where $l_m$is the mixing length and n can be solved by Eqs. (34) and (35).

Based on our experimenting condition (Wang et al., 2011), an empirical formula for estimating f_τ is described as:

$$f_\tau = 0.263u_l - 0.058 \tag{38}$$

where u_l is the liquid film velocity.

The total pressure gradient in churn flow, assuming the acceleration negligible, can be calculated as follows (Govan et al., 1991):

$$-\frac{dp}{dz} = \frac{4\tau_{wall}}{d_T} + (1-\alpha)\rho_l g + \alpha\rho_g g \tag{39}$$

where α is the void fraction. The equation for void fraction recommended by Hasan (1988) is adopted as:

$$\alpha = \frac{u_{sg}}{1.15u_m + 0.345\sqrt{gd_T(\rho_l - \rho_g)/\rho_l}} \tag{40}$$

$$u_m = u_{sg} + u_{sl} \tag{41}$$

where u_m is the mixture velocity.

Therefore, the dimensionless pressure gradient Δp^*can be expressed as:

$$\Delta p* = \left(-\frac{dp}{dz}\right)\frac{1}{(\rho_l - \rho_g)g} \tag{42}$$

2.2.5. Interfacial shear stress

Assuming that the gas flow is turbulent, the shear stress exerting on the windward side of the wave can be calculated as follows (Lin et al., 2005):

$$\frac{U_c}{v^*} = 2.5\ln\frac{\rho_c v^* r_{cal}}{\eta_g} + 1.75 \tag{43}$$

where r_{cal} is the calculating radius and $v^* = \sqrt{\tau_{ss}/\rho_c}$is the frictional velocity, respectively.

Since the velocity on the interface is parallel to the interface tangent, r_{cal}, rather than $d_T/2-\delta$, is taken here as the radius of the flow area, as is shown in Fig. 4. The variation of the shear stress in the gas phase next to the wave interface is shown in Fig. 5. It should be noticed that the interfacial shear stress along the windward side is obtained based on the above calculations, whereas the value on the leeward side is qualitative due to the flow separation. Because of the acceleration on the wave windward side, the absolute value of the shear stress reaches its maximum at the crest, and decreases to nearly zero just downstream the crest where the flow separation happens. In a

comparison of the shear stress with the gas pressure, the former is found to be about 6% of the latter. Therefore, the effect of the interfacial shear stress can be negligible, which confirms the hypothesis by Jayanti et al. (1996) and Da Riva and Del Col (2009).

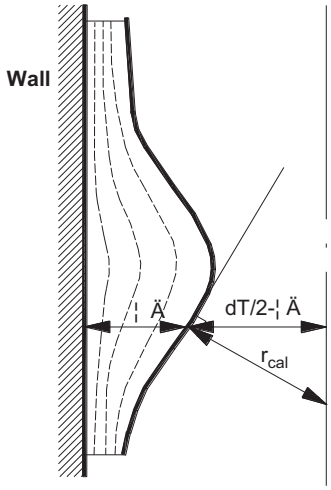

Fig. 4. Schematic of interfacial shear stress calculation.

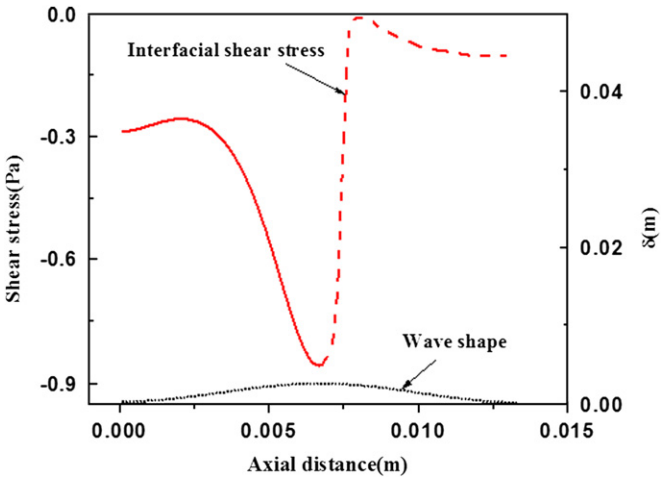

Fig. 5. Variation of shear stress on wave under critical condition.

2.3. Solving equations

As the forming process of the wave on the gas/liquid interface is ignored, the initial state of the wave has to be specified. The initial condition here is defined as a new wave with tiny amplitude (wave initial amplitude) generated on the liquid film when the resultant force acting on the control volume is equal to zero ($\Sigma F = 0$).

According to the experimental results, the wave forming at the liquid inlet continues growing until it reaches an amplitude big enough to be carried upwards. The critical condition for this reversal is that the wave velocity is equal to zero ($U_w = 0$).

Eqs. (9), (13), (14), and (15) are substituted into Eqs. (2), (3) to get the final expression for the mass and momentum conservation principles of the wave:

$$\frac{d}{dt}A_w = \frac{1}{C_1}\frac{\dot{M}_{LF,in}-\dot{M}_{LF,out}}{\rho_l} - \frac{C_3}{C_1}\frac{U_w}{3L_{sint}}\frac{\delta_{out}(\dot{M}_{LF,ss}-\dot{M}_{LF,out})}{\dot{M}_{LF,out}} - \frac{C_2}{C_1}\frac{U_w}{3L_{sint}}\frac{\delta_{in}(\dot{M}_{LF,ss}+\dot{M}_{LE}-\dot{M}_L)}{\dot{M}_{LF,in}} \tag{44}$$

$$V_w\frac{d}{dt}U_w + \frac{1}{2}\pi d_T L_w U_w \frac{d}{dt}A_w = \sum F + (U_{LF,in}\dot{M}_{LF,in} - U_{LF,out}\dot{M}_{LF,out}) \tag{45}$$

A four-order Runge–Kutta-type numerical method has been developed to solve Eqs. (4), (44), and (45) in time with the initial conditions described as follows:

$$\Sigma F = 0, \quad A_w(0) = A_0, \quad U_0 = u_l, \quad z(0) = 0 \tag{46}$$

3. Results and discussion

3.1. Model verification

Fig. 6 depicts the formation of a huge wave and its evolution which eventually leads to the liquid entrainment observed in our recent experimental study (Wang et al., 2011). The huge wave periodically forms at the bottom of the inlet section and grows in both the radial and axial directions. Due to the gravity, the wave

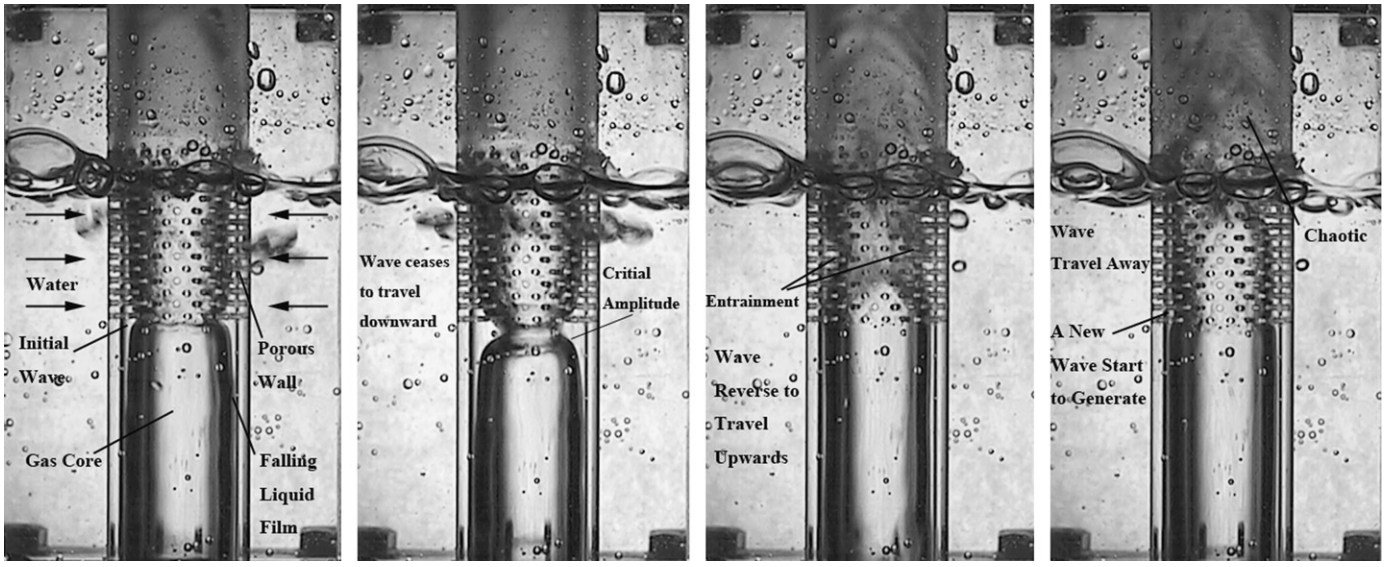

Fig. 6. Evolution of flooding waves in churn flow (Wang et al., 2011). ($u_{sg} = 6.17\ \mathrm{m\,s^{-1}}$, $u_{sl} = 7.49\times10^{-3}\ \mathrm{m\,s^{-1}}$, $U^* = 0.49$, $d_T = 19$ mm).

moves slightly down out of the porous-wall section till the wave reaches a critical amplitude for the flow reversal. The wave then starts to travel upwards and subsequently grows to a maximum amplitude before it departs from the inlet section.

A good agreement between the calculation results and experimental observations with regard to the wave behavior is qualitatively obtained in Fig. 7. Continually increasing of mass storage of control volume makes the wave amplitude growing until the mass flow rate leaving the control volume balances the entering. Gravity shows a significant effect in the early stage of the wave motion, making the huge wave move at first downwards due to the insufficient upward force. Subsequently, the downward absolute wave velocity deceases to zero, then the wave ceases to travel downwards and begin to travel upwards; meanwhile, the wave reaches its critical size.

A quantitative validation of the present model is also conducted by comparing the experimental wave amplitude in our study and the calculation results. The critical and the maximum amplitude of the wave are defined as the amplitude when the wave reverses, and the sum of the mass flow rate leaving out of the wave ($\dot{M}_{LF,out}$) and the entrained mass flow rate ($\dot{M}_{LE}$) balancing the mass flow rate flowing into the control volume ($\dot{M}_{LF,in}$), respectively. The measured critical amplitudes of the interfacial waves versus the predicted ones are plotted in Fig. 8, and the corresponding maximum amplitudes are given in Fig. 9. The experimental data are derived from the study by Wang et al. (2011) in a pipe with an internal diameter of 19 mm at the pressure approximate to the atmospheric pressure and under air/water churn flow condition. The superficial gas velocity ranges from 4.98 m s^{-1} to 12.75 m s^{-1}

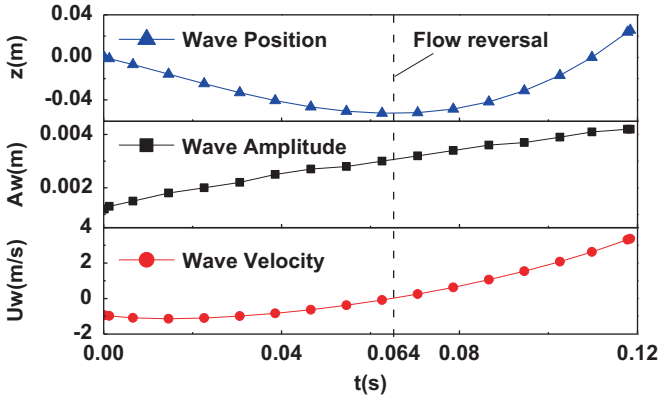

Fig. 7. A typical evolution of huge wave. (d_T=19mm, u_{sg}=8.03 m s^{-1}, u_{sl}=0.1 m s^{-1}).

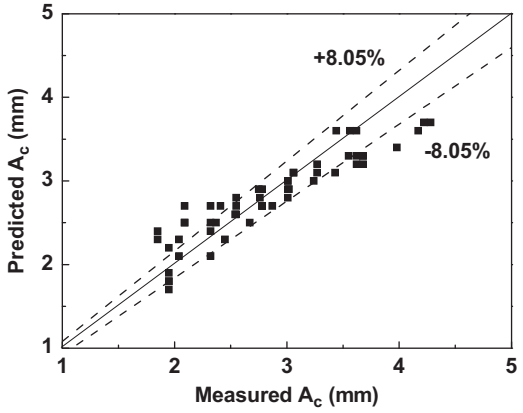

Fig. 8. Measured vs. predicted critical amplitude of interfacial waves. (d_T=19 mm, u_{sg}=4.98~12.75 m s^{-1}, u_{sl}=7.74×10^{-3}~1.48×10^{-1} m s^{-1}).

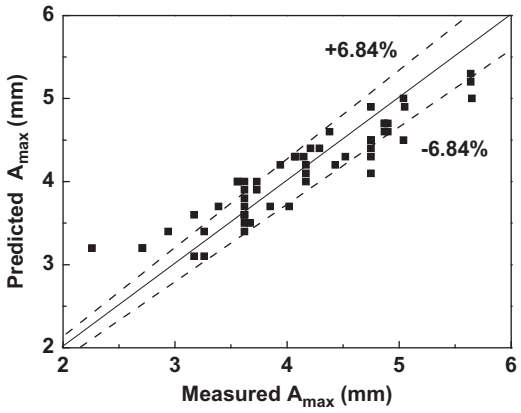

Fig. 9. Measured vs. predicted maximum amplitude of interfacial waves. (d_T=19 mm, u_{sg}=4.98~12.75 m s^{-1}, u_{sl}=7.74×10^{-3}~1.48×10^{-1} m s^{-1}).

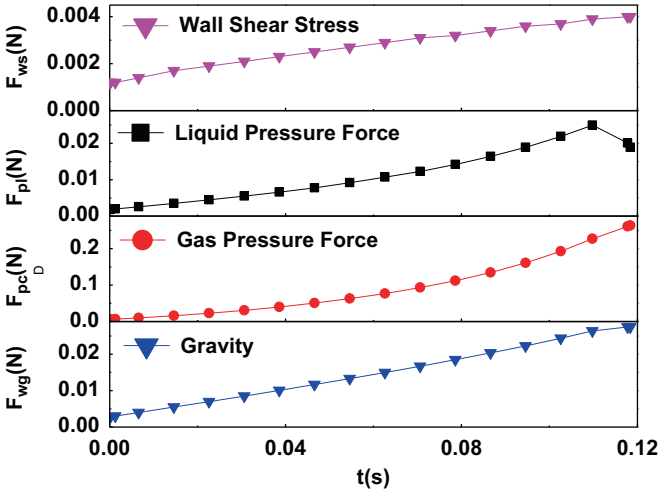

Fig. 10. Variation of forces with time. (d_T=19 mm, $\dot{M}_L$=28.47×10^{-3} kg s^{-1}, u_{sg}=8.03 m s^{-1}).

and the superficial liquid velocity ranges from 7.74×10^{-3} m/s to 1.48×10^{-1} m/s. With the proposed model, satisfactory predictions of both critical and maximum amplitudes are achieved over a large range of gas and liquid mass flow rates. The average absolute deviations in the predictions are 8.05% and 6.84%, respectively. Although the systematic errors in the experiment and the two major uncertainty sources (the assumption of the wave shape and the neglect of the wave deformation) inevitably affect the accuracy, the present model qualitatively and quantitatively reproduces the wave levitation process and the effects of the gas and liquid mass flow rates on the wave properties.

3.2. *Investigation of wave properties based on the model*

3.2.1. *Curves of the forces acting on the wave and pressure gradient*

More detailed analysis on the wave properties is made based on the experimental condition. Fig. 10 shows the variations of the forces acting on the control volume with the time. The results indicate that the gas pressure is the most important factor affecting the wave motion and the liquid pressure exerts non-negligible effect. It also can be inferred from the figure that the gravity and wall shear stress linearly change with the time, while the gas and liquid pressure increase non-linearly. It should be noted that when the top of the wave travels through the water inlet section, the water flowing into the control volume decreases,

which results in a slower growth in the gas pressure and gravity and a distinct decrease in the liquid pressure.

The pressure gradient distributions against the dimensionless gas velocity under churn flow condition are shown in Fig. 11. With the consistent trend as reported by Owen (1986), the pressure gradient decreases with the increase of the gas flow rate due to the decreasing intensity of the gas–liquid interaction, but increases with the increase of the liquid flow rate.

3.2.2. Wave movement under different flow conditions

The effects of the gas superficial velocity and the liquid mass flow rate on the wave trajectories are shown in Figs. 12 and 13, respectively. At a lower gas superficial velocity or a higher liquid mass flow rate, the huge waves have the tendency to travel longer distances due to the insufficient upward force. As the gas superficial velocity increases, the downward tendency is gradually restrained and the waves eventually flow upwards immediately when they enter into the annular flow. With the increasing liquid mass flow rate, the waves travel downwards more quickly but take shorter time to reverse. It also can be observed from the figure that the wave velocity increases with the increase of the gas velocity and the liquid mass flow rate.

3.2.3. Wave amplitude under different flow conditions

Only two main factors (the upward gas pressure and the downward gravity) exerting on the control volume are taken into account for the qualitative analysis on the huge wave amplitude. Fig. 14 shows the relationship between F_{pc}/F_{wg} and A_w/d_T at different dimensionless velocities U^*. Based on the above analysis, the initial condition can be simplified as $F_{pc}/F_{wg} \approx 1$ and the ratio of the pressure of the gas core to the gravity can be described as:

$$\frac{F_{pc}}{F_{wg}} \approx \frac{4\rho_g U_c^2 (d_T - A_w)^2}{5(\rho_l - \rho_g) d_T g (d_T - 2A_w)^2} \approx \frac{4}{5}(U^*)^2 \frac{[1-(A_w/d_T)]^2}{[1-2(A_w/d_T)]^2} \quad (47)$$

The result indicates that the wave amplitude increases with the increase of the pipe diameter. Moreover, in a specific pipe, the wave amplitude decreases with the increasing gas superficial velocity. The wave growth rate seems higher at a higher gas superficial velocity, while the wave amplitude asymptotically approaches a limiting value at a lower gas flow rate. In addition, as the dimensionless velocity U^* increases to about $U^* = 1.12$, the amplitude of the huge wave under the initial condition decreases to 0; therefore, it can be inferred that the huge wave disappears, which can be taken as the sign for the transition from the churn flow to the annular flow.

How the initial amplitude, the critical amplitude and the maximum amplitude of the huge wave are affected by the gas superficial velocities and the liquid mass flow rates under the experimental conditions are described in Figs. 15–17, respectively. It can be inferred from the figures that the initial amplitude is more affected by the gas phase and decreases with the increasing gas superficial velocity. The critical amplitude decreases with

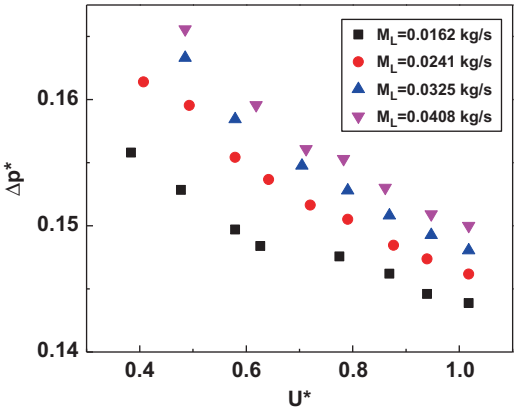

Fig. 11. The pressure gradient distribution against dimensionless gas velocity under churn flow condition.

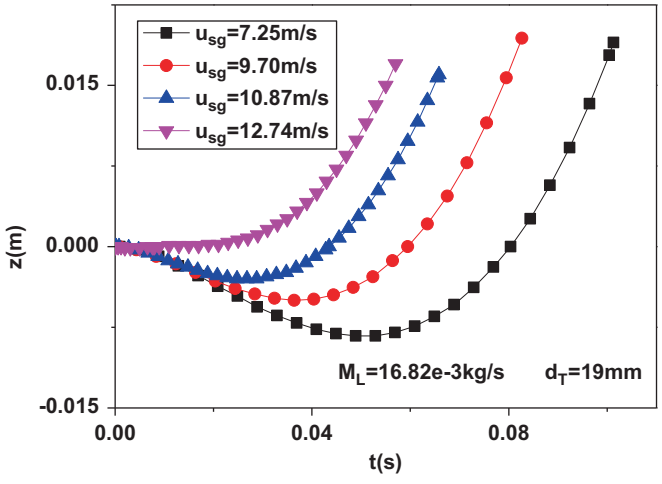

Fig. 12. Wave position at different gas flow rates with constant total liquid mass flow rate.

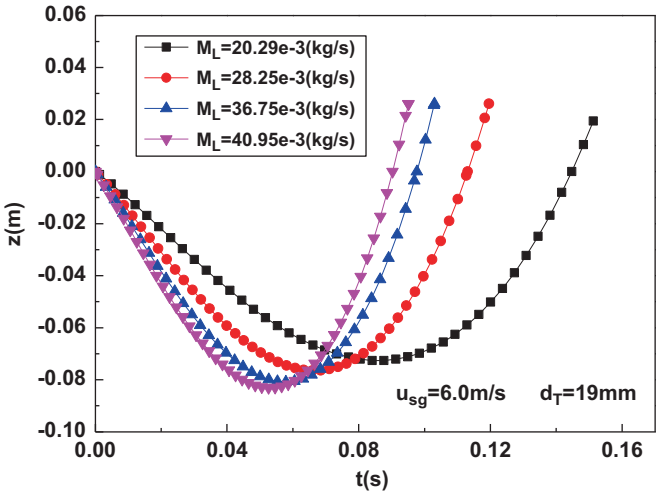

Fig. 13. Wave position at different liquid mass flow rates with constant total gas flow rate.

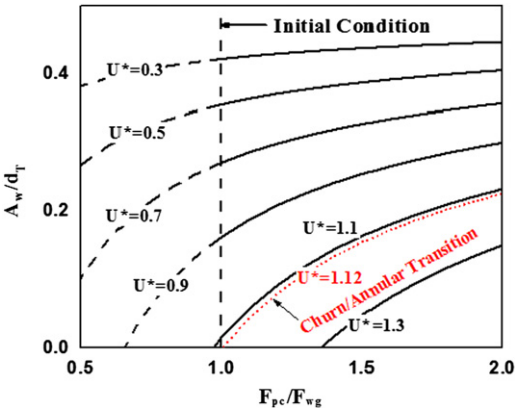

Fig. 14. F_{pc}/F_{wg} *vs.* A_w/d_T.

the increasing gas superficial velocity. At lower gas velocities, the critical amplitude at first increases with the increasing liquid mass flow rate and eventually asymptotically approaches a limiting value. The maximum amplitude, it decreases with the increasing gas mass flux, but increases with the increasing liquid mass flux. It appears that the entrainment imposes restrictions on the growth of the wave amplitude at higher gas and liquid flow rates.

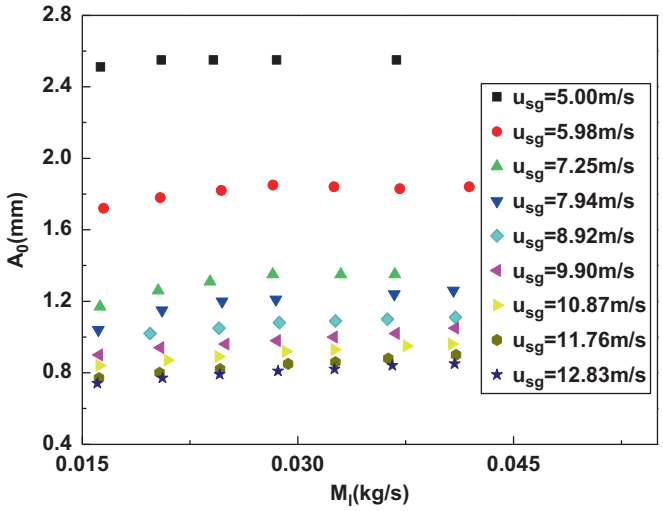

Fig. 15. Wave initial amplitude under different flow conditions.

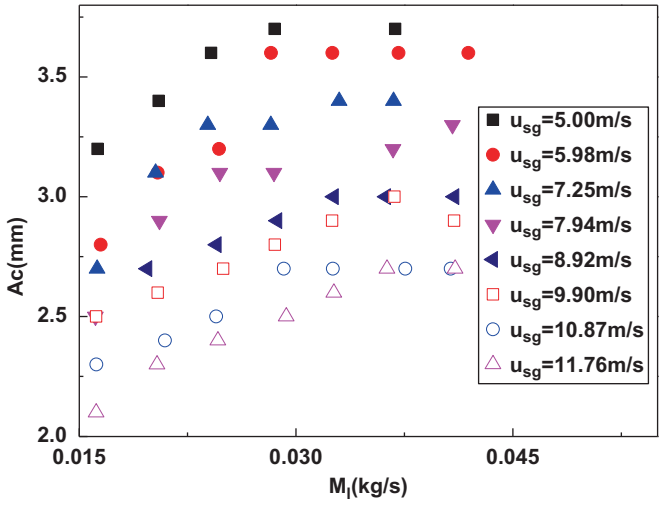

Fig. 16. Predicted critical amplitude of interfacial waves.

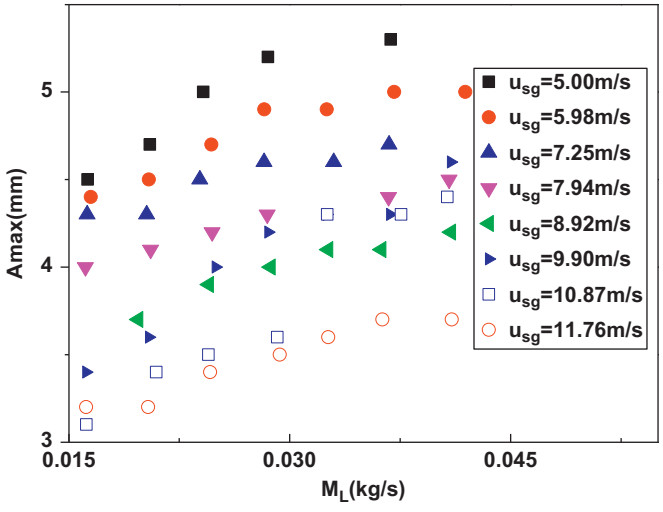

Fig. 17. Predicted maximum amplitude of interfacial waves.

4. Conclusions

Based on a fundamental analysis on the forces acting on the control volume, a physical model for the huge wave properties in churn flow was developed in this paper. We investigated in detail the impacts of the gravity, the pressure forces of the gas and liquid phase, the wall shear stress and the interfacial shear stress. And we depicted the detailed movement of the huge wave under the churn flow condition, reproduced the effects of the gas and liquid mass flow rates on the wave properties and predicted the transition from the churn flow to the annular flow. The proposed model was verified qualitatively and quantitatively over a range of experimental data obtained in our recent experimental study, with the average absolute deviations for critical amplitude (A_c) and maximum amplitude (A_{max}) of 8.84% and 6.97%, respectively. On the basis of our model, the flooding of the film was theoretically demonstrated as the overall characteristics of the regime. The flow reversal was attributed to the transition to the annular flow, which provides mechanistic insights into the distinction between the churn flow and the annular flow. The forces acting on the control volume and the pressure gradient were analyzed and the gas pressure was concluded as the most significant factor affecting the wave behavior. The wave properties (amplitude and velocity) which are crucial for the profound knowledge of the huge wave were also analyzed and the churn/annular transition occurred at $U^*=1.12$. Further studies with the assumption of a more accurate wave shape and the consideration of the wave deformation are expected to be covered in our future work.

Nomenclature

A	wave amplitude (mm)
d_T	pipe diameter (m)
E	entrained fraction
F	force (kg m s^{-2})
$\sum F$	resultant force (kg m s^{-2})
g	gravitational acceleration(m s^{-2})
G	volume flow rate (m^3 s^{-1})
L_{sint}	length of inlet section (m)
L_w	wave length (m)
$\dot{M}$	mass flow rate (kg s^{-1})
P	pressure (Pa)
ΔP	pressure drop (Pa)
r_{cal}	calculation radius (m)
S	area (m^2)
t	time (s)
u	superficial velocity (m s^{-1})
U	velocity (m s^{-1})
U^*	dimensionless superficial gas velocity
V	volume (m^3)
z	traveling distance (m)

Greek symbols

ρ	density (kg m^{-3})
τ	shear stress (kg m^{-1} s^{-2})
δ	film thickness (m)
σ	surface tension (N m^{-1})
η	viscosity (kg s^{-1} m^{-1})

Subscripts

c	gas core
crest	wave crest
g	gas phase
in	enter the control volume
l	liquid phase
lam	laminar
LF	liquid film
out	leave the control volume
tur	turbulent
wall	wall
w	wave

Acknowledgments

This work was financially supported by the National Nature Science Foundation of China for Creative Research Groups under the Contract No. 51121092.

References

Ahmad, M., Peng, D.J., Hale, C.P., Walker, S.P. and Hewitt, G.F., 2010. Drop Entrainment in Churn Flow. 7th International Conference on Multiphase Flow, Tampa, FL, USA.

Assad, A., Jan, C., Lopez de Bertodano, M., Beus, S., 1998. Scaled experiments in ripple annular flow in a small tube. Nucl. Eng. Des. 184, 437–447.

Azzopardi, B.J., Wren, E., 2004. What is entrainment in vertical two-phase churn flow? Int. J. Multiphase Flow 30, 89–103.

Barbosa, J., Govan, A.H., Hewitt, G.F., 2001. Visualization and modeling studies of churn flow in a vertical pipe. Int. J. Multiphase Flow 27 (12), 2105–2127.

Da Riva, E., Del Col, D., 2009. Numerical simulation of churn flow in a vertical pipe. Chem. Eng. Sci. 64 (17), 3753–3765.

Govan, A.H., Hewitt, G.F., Richter, H.J., Scott, A., 1991. Flooding and churn flow in vertical pipes. Int. J. Multiphase Flow 17, 27–44.

Han, H., Zhu, Z., Gabriel, K., 2006. A study on the effect of gas flowrate on the wave characteristics in two-phase gas–liquid annular flow. Nucl. Eng. Des. 236, 2580–2588.

Hasan, A.R., 1988. Void fraction in bubbly, slug and churn flow in vertical two-phase up-flow. Chem. Eng. Commun. 66, 101–111.

Hazuku, T., Takamasa, T., Matsumoto, Y., 2008. Experimental study on axial development of liquid film in vertical upward annular two-phase flow. Int. J. Multiphase Flow 34, 111–127.

Hewitt, G.F., Hall-Taylor, N., 1970. Chapter 2, Annular Two-Phase Flow. Pergamon Press, Oxford.

Hewitt, G.F., Jayanti, S., 1993. To churn or not to churn. Int. J. Multiphase Flow 19 (3), 527–529.

Hewitt, G.F., Martin, C.J., Wilkes, N.S., 1985. Experimental and modelling studies of annular flow in the region between flow reversal and the pressure drop minimum. PhysicoChem Hydrodyn 6 (1/2), 69–86.

Holowach, M.J., Hochreiter, L.E., Cheung, F.B., 2002. A model for droplet entrainment in heated annular flow. Int. J. Heat Fluid Flow 23, 807–822.

Jayanti, S., Hewitt, G.F., 1992. Prediction of the slug-to-churn flow transition in vertical two-phase flow. Int. J. Multiphase Flow 18 (6), 847–860.

Jayanti, S., Hewitt, G.F., Low, D.E.F., Hervieu, E., 1993. Observation of flooding in the Taylor bubble of co-current upwards slug flow. Int. J. Multiphase Flow 19 (3), 531–534.

Jayanti, S., Tokarz, A., Hewitt, G.F., 1996. Theoretical investigation of the diameter effect on flooding in countercurrent flow. Int. J. Multiphase Flow 22, 307–324.

Lin, J.Z., Ruan, X.D., Chen, B.G., Wang, J.P., Zhou, J., Ren, A.L., 2005. Chapter 6, Fluid Mechanic. Tsinghua University Press, Beijing in Chinese.

McQuillan, K.W., Whalley, P.B., Hewitt, G.F., 1985. Flooding in vertical two-phase flow. Int. J. Multiphase Flow 11, 741–760.

Munson, B.R., Young, D.F., Okiish, T.H., 1990. Fundaments of Fluid Mechanics. John wiley & sons, New York.

Nusselt, W., 1916. Surface Condensation of Water. Z. Ver. Dtsch. Ing. 60 (26), 541–546. 569-575; 60 (27).

Omebere-Iyari, N.K., Azzopardi, B.J., 2007. A study of flow patterns for gas/liquid flow in small diameter tubes. Chem. Eng. Res. Des. 85, 180–192.

Owen, D.G., 1986. An Experimental and Theoretical Analysis of Equilibrium Annular Flows. Ph.D. Thesis. University of Birmingham. UK.

Sekoguchi, K., Takeishi, M., 1989. Interfacial structures in upward huge wave flow and annular flow regimes. Int. J. Multiphase Flow 15, 295–305.

Shearer, C.J., Davidson, J.F., 1965. The investigation of a standing wave due to gas blowing upwards over a liquid filml its relation to flooding in wetted wall columns. J. Fluid Mech. 22 (2), 321–335.

Taitel, Y., Barnea, D., Dukler, A.E., 1980. Modelling of flow pattern transitions for steady upward gas–liquid flow in vertical tubes. A.I.Ch.E. J 26, 345–354.

Wallis, G.B., 1969. Chapter 7, One-Dimensional Two-Phase Flow. McGraw-Hill, New York 11.

Wang, K. Bai B.F., Yang, B., Xie, C., 2011. Properties of Interfacial Waves in Vertical Churn Flow. 14th International Topical Meeting on Nuclear Reactor Thermal-hydraulics. Toronto, Ontario, Canada.

Wang, Z.L., Gabriel, K.S., Manz, D.L., 2004a. The influences of wave height on the interfacial friction in annular gas–liquid flow under normal and microgravity conditions. Int. J, Multiphase Flow 30, 1193–1211.

Wang, Z.L., Gabriel, K.S., Zhu, Z.F., 2004b. The effects of gravity on the features of the interfacial waves in annular two-phase flow. Microgravity Sci. Technol. XV (3), 19–27.

Zuber, N., Findlay, J.A., 1965. Average volumetric concentration in two-phase flow systems. J. Heat Transfer 87, 453–468.